

Electron-Phonon Coupling in Boron-Doped Diamond Superconductor

H. J. Xiang, Zhenyu Li, Jinlong Yang, J. G. Hou, and Qingshi Zhu

Hefei National Laboratory for Physical Sciences at Microscale,
Laboratory of Bond Selective Chemistry and Structure Research Laboratory,
University of Science and Technology of China,
Hefei, Anhui 230026, People's Republic of China

(Dated: January 27, 2020)

Abstract

The electronic structure, lattice dynamics, and electron-phonon coupling of the boron-doped diamond are investigated using the density functional supercell method. Our results indicate the boron-doped diamond is a phonon mediated superconductor, confirming previous theoretical conclusions deduced from the calculations employing the virtual crystal approximation. We show that the optical phonon modes involving B vibrations provide most of the electron-phonon coupling. Different from previous theoretical results, our calculated electron-phonon coupling constant is 0.39 and the estimated superconducting transition temperature T_c is 4.4 K for the boron doped diamond with 2.78% boron content using the Coulomb pseudopotential $\mu^* = 0.10$, in excellent agreement with the experimental result.

PACS numbers: 74.25.Kc, 74.25.Jb, 74.70.Ad, 74.62.Dh

Recently, Ekimov et al.¹ reported the discovery of superconductivity in the boron-doped diamond synthesized at high pressure and high temperature. Their measurements showed that the boron-doped diamond with a hole carrier density of $5 \times 10^{21} \text{ cm}^{-3}$ is a bulk, type-II superconductor below the superconducting transition temperature $T_c = 4 \text{ K}$. Using a simplified McMillan formula² by setting the Coulomb pseudopotential to zero, they estimated the electron-phonon coupling constant $\lambda = 0.2$, indicative of weak electron-phonon coupling.

Before that, a few superconducting semiconductors have been discovered experimentally,^{3,4} and superconductivity in many-valley degenerate semiconductor was also predicted theoretically.⁵ As the first group-IV diamond type superconducting semiconductor, the boron-doped diamond superconductor has been studied by several groups. Baskaran et al.⁶ suggested a resonating valence bond (RVB)⁷ mechanism of impurity band superconductivity in diamond. When the boron doping concentration increases to a critical value $n_c = 4 \times 10^{21} \text{ cm}^{-3}$, an Anderson-Mott insulator to RVB superconductivity transition takes place. By first principles density functional perturbation calculations⁸ employing the virtual crystal approximation (VCA),⁹ Boeri and co-workers¹⁰ substantiated that the recently discovered superconductivity below 4 K in 3% boron-doped diamond is caused by the coupling of a few holes at top of the σ -bonding valence band to the optical zone-center phonons, similar as in MgB_2 ,^{11,12,13,14} albeit in 3 dimensions. Another first principles study employing the VCA and frozen phonon method also indicated that the electron-phonon coupling is the likely superconducting mechanism.¹⁵ Regardless of their similar conclusion in these two studies, we note that there are some discrepancies in these two studies, especially in the electron-phonon coupling strength and T_c : $\lambda = 0.27$ and $T_c = 0.2 \text{ K}$ when the Coulomb pseudopotential $\mu = 0.10$ for 3% doping concentration in the first study, however, $\lambda = 0.55$ and $T_c = 9 \text{ K}$ when $\mu = 0.15$ for 2.5% doping concentration in the second study. The difference in doping concentration makes the discrepancy even more prominent since larger doping concentration leads to larger λ and T_c . Moreover, though qualitative agreement with experiment is found in these two studies, some obvious disagreements still exist, in particular, T_c in the first study is too small, and T_c in the second study is too large though one can obtain $T_c = 4 \text{ K}$ by setting μ to a somewhat large value, i.e., 0.20. The disagreements between experiment and theory might indicate the inapplicability of the VCA to the newly found boron-doped diamond superconductor, since there are some

cases where the VCA failed, e.g., the VCA was inappropriate for calculating the band gaps of GaPN and GaAsN,¹⁶ and it described badly the structural and electronic properties of the quaternary alloy GaInAsN.¹⁷ On the other hand, though computationally demanding, the supercell method is usually reliable.^{16,17} To bridge the gap between experiment and theory, and to verify the phonon mediated superconducting mechanism in the boron-doped diamond, here we report a first principles supercell calculation on the electron-phonon coupling of the boron-doped diamond. Our results support the conventional phonon mediated superconducting mechanism in boron-doped diamond and the calculated T_c is in excellent agreement with the experimental value.

Electronic structure calculations and geometrical optimizations are performed using density functional theory (DFT)^{18,19} in the local density approximation (LDA).^{20,21} The electron-ion interaction is described by ultrasoft Vanderbilt-type pseudopotentials,²² which allow a low cutoff energy (25 Ry in this work) in the plane-wave expansion. The phonon and electron-phonon coupling calculations are carried out using density functional perturbation theory in the linear response.⁸ Within the phonon mediated theory of superconductivity, T_c can be estimated using McMillan's solution of the Eliashberg equation,²

$$T_c = \frac{\lambda_{\ln}^{\text{ph}}}{1.20} \exp \left[-\frac{1.04(1 + \mu^*)}{1 + 0.62 \mu^*} \right]; \quad (1)$$

where λ is the electron-phonon coupling constant, $\lambda_{\ln}^{\text{ph}}$ is the logarithmically averaged characteristic phonon frequency, and μ^* is the Coulomb pseudopotential which describes the effective electron-electron repulsion. The electron-phonon coupling is calculated as an average over the N_{q} points mesh and over all the phonon modes, $\lambda = \frac{1}{N_{\text{q}}} \sum_{\text{q}} \lambda_{\text{q}}$, where λ_{q} is the electron-phonon interaction for a phonon mode with momentum q . The modes responsible for superconductivity can be identified from the Eliashberg function,

$${}^2F(\omega) = \frac{1}{2N} \sum_{\text{q}} \omega_{\text{q}}^2 \lambda_{\text{q}}(\omega - \omega_{\text{q}}): \quad (2)$$

Then the logarithmically averaged characteristic phonon frequency is calculated as,

$$\lambda_{\ln}^{\text{ph}} = \exp \left[\frac{2}{\omega_0} \int_0^{\omega_D} \omega {}^2F(\omega) \ln \omega d\omega \right]; \quad (3)$$

We use the supercell technique to model the boron-doped diamond. In order to study the dependence of the electron-phonon coupling on the doping concentration, we choose two models: $2 \times 2 \times 2$ and $3 \times 3 \times 2$ diamond supercells with a carbon atom substituted by a

boron atom, namely models I and II respectively. The total B content (C_B) for experimental samples is 2.8–3.0%, which is smaller than the total B content (6.25%) in model I and very close to the total B content (2.78%) in model II. The two models are shown in Fig 1. The optimized lattice constant for diamond is 3.57 Å, agreed well with the experimental lattice constant (3.566 Å)¹ and previous theoretical results.²³ For the boron-doped diamond we check that our calculations reproduce the slight lattice expansion, less than 0.3%.¹ Since the not very large boron doping has negligible effect on the lattice constant of diamond, we use our optimized lattice constant (3.57 Å) in all subsequent calculations.

The k-point integration for geometrical optimization, construction of the induced charge density, and calculation of the dynamical matrix is performed over a $4 \times 4 \times 4$ ($2 \times 2 \times 3$) Monkhorst-Pack grid²⁴ for model I (II), and a finer $8 \times 8 \times 8$ ($4 \times 4 \times 6$) grid is used in the phonon linewidth calculations where the convergence in the k-point sampling is more difficult than that for the phonon calculations. The dynamical matrix and phonon linewidth have been computed on a $3 \times 3 \times 3$ ($2 \times 2 \times 3$) q-point mesh for model I (II), and a Fourier interpolation has been used to obtain complete phonon dispersions.

The total electronic density of states (TDOS) and local density of states (LDOS) for models I and II are plotted in Fig 2 (The TDOS for the undoped diamond is also shown as a reference). The TDOS clearly indicates a degenerate or metallic behavior in both models, contrasting sharply to the semiconductor behavior of the undoped diamond. The TDOS and LDOS for model I are very similar with those for model II except that the width of the acceptor bands (the bands between the valence top and the Fermi level) for model I is larger than that for model II. For both cases, the width of the acceptor bands is larger than that for a boron-doped diamond 64-atom supercell, obtained by Bamardiy et al.,²⁵ suggesting a dependence of the width of the acceptor bands on the boron doping concentration. When the doping concentration decreases, the width of the acceptor bands decreases. At very small doping concentration, the acceptor bands even no longer overlap with the valence band edge of the diamond resulting in a threefold degenerate acceptor state with a hole binding energy of $E_B = 0.37$ eV.²⁶ The metallization in the boron-doped diamond is reasonably caused by the increased boron content, doesn't necessarily resort to the Anderson impurity model²⁷ as suggested by Pogorelov et al.²⁸ Fig 2 (b) and (c) contain the LDOS plots of the boron atom and one of the four C atoms nearest to B. The LDOS for other C atoms differ only a little for the C LDOS shown here. From Fig 2 we can clearly see that the LDOS around

the Fermi level for B is larger than that for the selected C atom. However, it doesn't mean the electronic states near the Fermi level are localized around B since the sum of the LDOS for all C atoms is larger than the LDOS for B.

The calculated frequency of the highest optical phonon at Γ for the updoped diamond is 1295 cm^{-1} , agreed well with previous LDA calculations,^{10,23} a little smaller than experimental frequency, 1332 cm^{-1} .¹ The phonon band structures for the undoped and boron-doped $2 \times 2 \times 2$ diamond supercell are shown in Fig 3 (a) and (b) respectively. Here, we plot the phonon band structure for the diamond supercell just for comparison with that for the boron-doped diamond. The phonon band structure for the diamond supercell is more complex than that for the unit cell since there are much more carbon atoms in the supercell. There are more lines for the boron-doped diamond since some phonon degenerates are removed due to the symmetry breaking. Beside that, a general effect to the phonon band structures resulting from the boron doping is the phonon softening. Especially the softening of the optical phonons is sizeable, e.g., the highest frequency of the zone center optical phonons decreases 99 cm^{-1} to 1196 cm^{-1} . We can see that there is a slight upturn of the uppermost mode especially when moving from Γ to X for both updoped and doped diamond, similar to the previous results,^{23,29} moreover, the upturn for the boron-doped diamond is more noticeable due to the larger electron-phonon coupling for the zone center optical phonons.

The phonon density of states (DOS) for both models is shown in the upper panels of Fig 4. The shapes of the phonon DOS for these two models are very similar except that the phonon softening effect in model I is stronger due to the larger boron concentration. The lower panels of Fig 4 are the Eliashberg function $\alpha^2F(\omega)$ and the boron partial phonon DOS for both models. The extremely weak signal in the low frequency part (lower than 80 meV) of $\alpha^2F(\omega)$ indicates very weak electron acoustic phonon coupling. The strongest peak of $\alpha^2F(\omega)$ for model I doesn't correspond to that of the total phonon DOS, but near the strongest peak for the boron partial phonon DOS. For model II, a strong double peak is prominent in $\alpha^2F(\omega)$ with a peak corresponding to the peak of the total phonon DOS. The large similarity in shape between the boron partial phonon DOS and $\alpha^2F(\omega)$ suggests the significant role of the boron vibrations in the electron-phonon coupling. However, this doesn't mean that only boron vibrations contribute to the electron-phonon coupling since all the vibrational modes are delocalized and no localized boron vibration exists due to the little mass difference between boron and carbon. Comparing our calculated $\alpha^2F(\omega)$ with those

obtained by Boeri et al.,¹⁰ we find that ${}^2F(\Gamma_2)$ has sizeable contributions from phonons with medium frequency in our results, however, in their result ${}^2F(\Gamma_2)$ vanishes for phonon frequencies below that of the optical zone-center modes, then jumps to a maximum, and finally falls.¹⁰ Their relative simple picture for ${}^2F(\Gamma_2)$ should stem from the fact that there are only three optical phonon modes in their virtual crystal calculations. Since we involve much more phonon modes to calculate ${}^2F(\Gamma_2)$, our results should be more reliable.

The calculated TDOS at the Fermi level ($N(E_F)$), average frequencies ω_{in}^{ph} , electron-phonon coupling constants λ , and superconducting transition temperatures T_c for model I and II are listed in Table I. As expected, the $N(E_F)$ for model I is larger than that for model II due to the larger boron concentration. The $N(E_F)$ for the boron-doped diamond is consistent with the virtual crystal calculations: $N(E_F)$ (in states/(spin eV diamond unit cell)) is 0.062 for 2.78% boron vs 0.060 for 2.5% boron,¹⁵ 0.106 for 6.25% boron vs 0.08 for 5% boron.¹⁰ The smaller $N(E_F)$ for the boron-doped diamond than MgB_2 would result in weaker electron-phonon coupling in the boron-doped diamond. The large ω_{in}^{ph} for the boron-doped diamond leads to high T_c , as demonstrated in McMillan's formula.² Though the phonon softening increases with increased boron concentration, ω_{in}^{ph} for model I is larger than that for model II, i.e., 1287 K vs 1218 K. The smaller ω_{in}^{ph} for model II results from the substantial electron-phonon coupling in the medium frequency region. The electron-phonon coupling constant for model I is 0.56, larger than that ($\lambda = 0.39$) for model II. The typical value for λ is in the range 0.10 to 0.15. The calculated T_c for model I is 23.6 (11.5) K for $\lambda = 0.10$ (0.15), and for model II it is 4.4 (0.9) K for $\lambda = 0.10$ (0.15). The boron concentration for model II is very close to the experimental value and the calculated T_c agrees well with experimental T_c , about 4 K. We can see T_c increases with increased boron concentration due to the increased λ . Detailed analysis reveals that the electron-phonon coupling is peaked at Γ_2 , which is also found in previous study.¹⁰ Lee et al.¹⁵ overestimated λ and T_c since the electron-phonon coupling constant should be averaged over the whole BZ, but their frozen phonon calculations only took into account the zone center phonons.

Our treatment neglects the anharmonic corrections. For MgB_2 , Choiet al.¹³ showed that λ is decreased from 1.0 to 0.78 after including partial anharmonic corrections. However, more recently, Lazzeri et al.¹⁴ suggested that the effects of anharmonicity on T_c and λ in MgB_2 are indeed negligible by explicitly taking into account the scattering between different phonon modes at different q points in the whole BZ. Boeri et al.¹⁰ considered the anharmonic

corrections in the boron-doped diamond using frozen phonon calculations and found that the effect of anharmonicity is small, i.e., in general decreases 0.03 after taking into account the anharmonicity. So our main results remain essentially unchanged even after including the anharmonic corrections since the anharmonic corrections for the boron-doped diamond are small, as discussed by Lee et al.¹⁵

In summary, we have carried out a first principles study on the heavily boron-doped diamond. Optical phonons in diamond are softened after doped with boron. The Eliashberg function $^2F(\omega)$ is mainly contributed by the boron related vibrational modes. Superconductivity in the boron-doped diamond is found to be mediated by the electron-phonon coupling. By using the supercell technique, we resolve the discrepancy between theoretical results based on the VCA and experimental data, and the calculated T_c is in excellent agreement with the experimental result.

This work is partially supported by the National Project for the Development of Key Fundamental Sciences in China (G1999075305, G2001CB3095), by the National Natural Science Foundation of China (50121202, 20025309, 10074058), by the Foundation of Ministry of Education of China, by the Foundation of the Chinese Academy of Science, and by the USTC-HP HPC project.

Corresponding author. E-mail: jlyang@ustc.edu.cn

- ¹ E. A. Ekimov, V. A. Sidorov, E. D. Bauer, N. N. Mel'nik, N. J. Curro, J. D. Thompson, and S. M. Stishov, *Nature (London)* 428, 542 (2004).
- ² W. L. McMullan, *Phys. Rev.* 167, 331 (1968).
- ³ J. F. Schooley, W. R. Hosler, and M. L. Cohen, *Phys. Rev. Lett.* 12, 474 (1964).
- ⁴ R. A. Hein and E. M. Swiggard, *Phys. Rev. Lett.* 24, 53 (1970).
- ⁵ M. L. Cohen, *Phys. Rev.* 134, A 511 (1964).
- ⁶ G. Baskaran, cond-mat/0404286.
- ⁷ P. W. Anderson, *Science* 235, 1196 (1987).
- ⁸ S. Baroni, S. de Gironcoli, A. Dal Corso, and P. Giannozzi, *Rev. Mod. Phys.* 73, 515 (2001); S. Baroni, A. Dal Corso, S. de Gironcoli, and P. Giannozzi, <http://www.pwscf.org>.
- ⁹ L. Nordheim, *Ann. Phys. (Leipzig)* 9, 607 (1931).

- ¹⁰ L. Boeri, J. Kortus, and O. K. Andersen, cond-m at/0404447.
- ¹¹ J. Nagamatsu, N. Nakagawa, T. Muranaka, Y. Zenitani, and J. Akimitsu, Nature (London) 410, 63 (2001).
- ¹² J. Man, W. E. Pickett, Phys. Rev. Lett. 86, 4366 (2001).
- ¹³ H. J. Choi, D. Roundy, H. Sun, M. L. Cohen, and S. G. Louie, Nature (London) 418, 758 (2002); Phys. Rev. B 66, 020513(R) (2002).
- ¹⁴ M. Lazzeri, M. Calandra, and F. Mauri, Phys. Rev. B 68, 220509(R) (2003).
- ¹⁵ K.-W. Lee, W. E. Pickett, cond-m at/0404547.
- ¹⁶ L. Bellaiche, S.-H. Wei, and A. Zunger, Appl. Phys. Lett. 70, 3558 (1997).
- ¹⁷ C. Chen, E. G. Wang, Y. M. Gu, D. M. Bylander, and L. Kleinman, Phys. Rev. B 57, 3753 (1998)
- ¹⁸ P. Hohenberg and W. Kohn, Phys. Rev. 136, B864 (1964).
- ¹⁹ W. Kohn and L. J. Sham, Phys. Rev. 140, A1133 (1965).
- ²⁰ D. M. Ceperley and B. J. Alder, Phys. Rev. Lett. 45, 566 (1980).
- ²¹ J. P. Perdew and A. Zunger, Phys. Rev. B 23, 5048 (1981).
- ²² D. Vanderbilt, Phys. Rev. B 41, 7892 (1990).
- ²³ N. Vast and S. Baroni, Phys. Rev. B 61, 9387 (2000).
- ²⁴ H. J. Monkhorst and J. D. Pack, Phys. Rev. B 13, 5188 (1976).
- ²⁵ A. S. Bamard, S. P. Russoz, and I. K. Snook, Philos. Mag. 83, 1163 (2003).
- ²⁶ F. Fontaine, J. Appl. Phys. 85, 1409 (1999).
- ²⁷ P. W. Anderson, Phys. Rev. 124, 41 (1961).
- ²⁸ Yu. G. Pogorelov and V. M. Loktev, cond-m at/0405040.
- ²⁹ M. Schworer-Bohning, A. T. Macrander, and D. A. Rams, Phys. Rev. Lett. 80, 5572 (1998).

TABLE I: Computed electronic DOS at the Fermi level ($N(E_F)$), average frequencies $\omega_{\text{ln}}^{\text{ph}}$, electron-phonon coupling constants λ , and superconducting transition temperatures T_c for models I and II. The two values for T_c correspond to two different values of λ (0.10 and 0.15). $N(E_F)$ is in states/(spin eV diam ond unit cell). Boron content C_B is also shown for each model.

	C_B	$N(E_F)$	$\omega_{\text{ln}}^{\text{ph}}$ (K)	λ	T_c (K)
Model I	6.25%	0.106	1287	0.56	23.6, 11.5
Model II	2.78%	0.062	1218	0.39	4.4, 0.9

FIG .1: (Color online) Structures of (a) model I and (b) model II. Refer to the text for the description for the models.

FIG .2: (Color online) Electronic DOS for the undoped diamond and two boron-doped diamond models. (a) shows the TDOS of the undoped diamond, (b) and (c) are the TDOS and LDOS plots for models I and II. The LDOS for C shown here represents the LDOS of one of the C atoms nearest to B. TDOS is in states/(spin eV diamond unit cell). The unit of LDOS is states/(eV supercell). Energy is relative to the Fermi level E_F (for the undoped diamond, the valence top is taken as zero energy point).

FIG .3: Phonon band structures for (a) $2 \times 2 \times 2$ supercell diamond and (b) $2 \times 2 \times 2$ supercell diamond with a carbon atom substituted by a boron atom (model I).

FIG .4: (Color online) Total phonon DOS, Eliashberg function $^2F(\omega)$, and boron partial phonon DOS for (a) model I and (b) model II. Total and partial phonon DOS shown here are in arb. units.

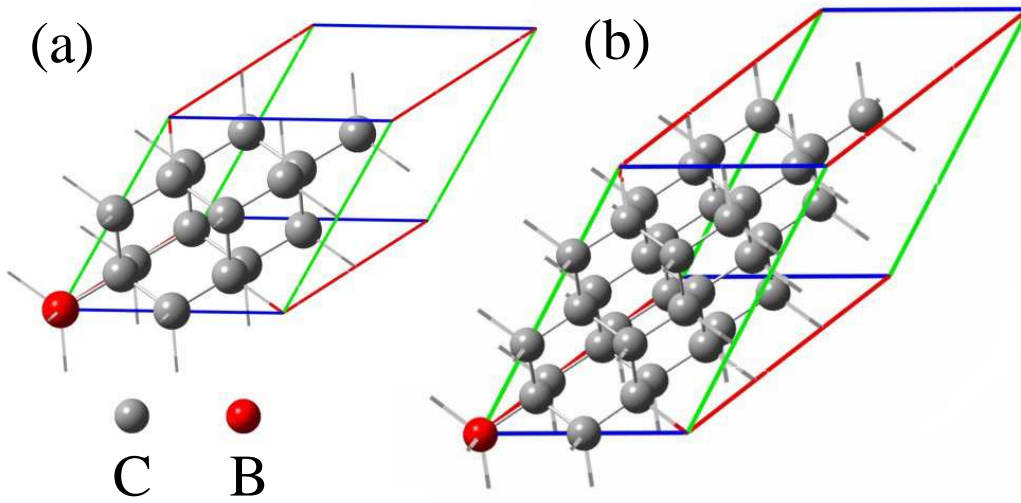


Fig. 1 of Xiang et al.

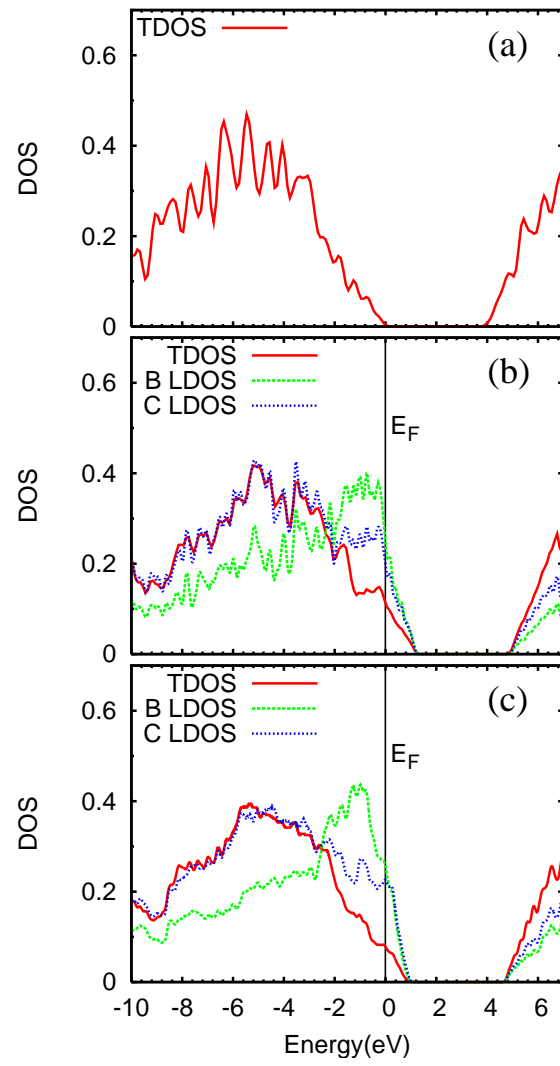


Fig. 2 of Xiang et al.

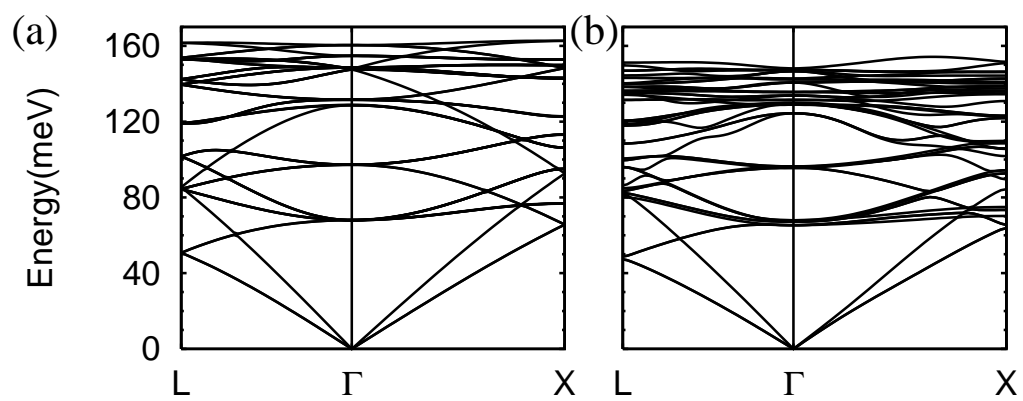


Fig. 3 of Xiang et al.

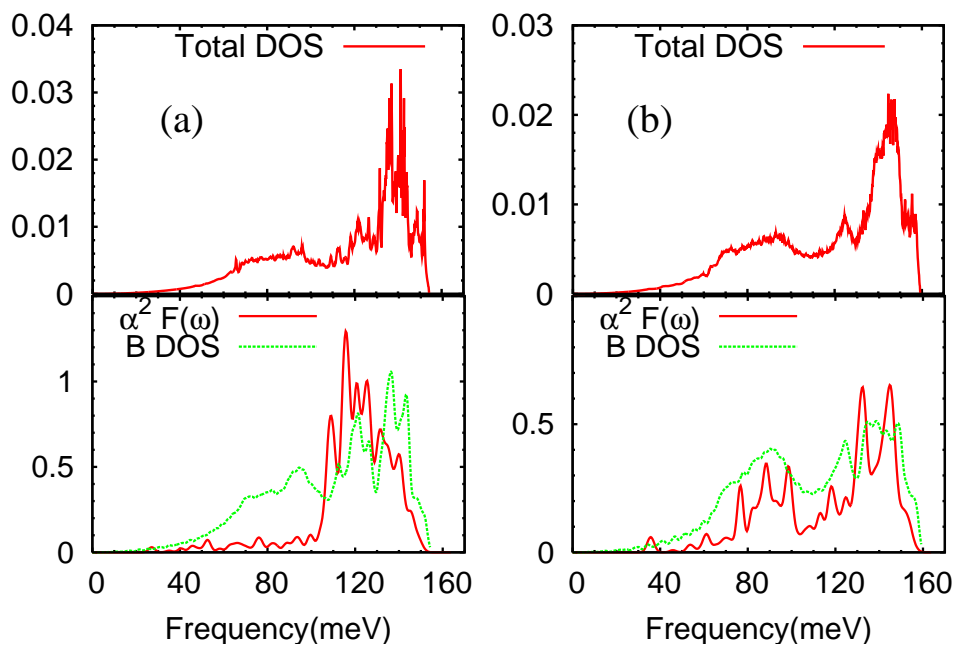


Fig. 4 of Xiang et al.